[5] Willmarth, W. W., Hawk, N. E., and Harvey, R. L., "Steady and Unsteady Motions and Wakes of Freely Falling Disks," *The Physics of Fluids*, Vol. 7, No. 2, Feb. 1964, pp. 197–208.

[6] Magarvey, R. H. and Blackford, B. L., "Wake Metamorphism Behind a Sphere," *Canadian Journal of Physics*, Vol. 40, 1962, pp. 1036–1040.

Tests of Cylindrical Shell under Concentrated Loads Applied to a Reinforcing Ring

ARNOLD ALLENTUCH,* KEVIN BRADY,† EUGENE GOLUB,‡ AND JOSEPH KEMPNER§
Polytechnic Institute of Brooklyn, Brooklyn, N. Y.

Introduction

ENGINEERS involved in the fields of submarines, missiles, aircraft, and pressure vessels use reinforced shells so extensively that investigations in this area are of continuing interest. For example, the stress analysis problem of a pressurized circular cylindrical shell reinforced by rings, one or more of which is externally loaded, is important in design considerations. In this Note, the authors provide experimental verification of the results from a previously obtained solution[1] of the closely related problem of a long circular cylindrical shell reinforced at its midlength by a single ring. Applied at the ends of a diameter of the ring are two self-equilibrating concentrated outward radial forces in the plane of the ring.

Curves showing stress distributions and displacements in the cylinder, obtained analytically and experimentally, are presented for a particular combination of ring and shell parameters.

Analytic Solution

The theoretical solution to the problem of an infinite shell, reinforced at its midlength by diametrically loaded rings, has been obtained by Allentuch, Brady, and Kempner.[1] In that solution they used the Donnell shell equations[2] with appropriate solutions given by Hoff[3] and Pohle and Nardo[4] to analyze the shell. The experiment under consideration in this Note was designed to verify some of the unusual results obtained in Ref. 1.

Experimental Setup

An experiment was designed to determine the stresses in and displacements of a long circular cylindrical shell reinforced at its midpoint by a single uniform ring. Applied to the opposite ends of a diameter of the ring were two equal concentrated outward radial loads.

The results obtained from the analytical solution[1] indicated that the maximum radial deflection of the shell did not occur at the ring. They further showed that the eccentricity e, between the ring and shell centerlines, had a first-order effect on the stresses in and displacements of the cylinder. These effects are not encountered in reinforced cylinders that deform axisymmetrically.

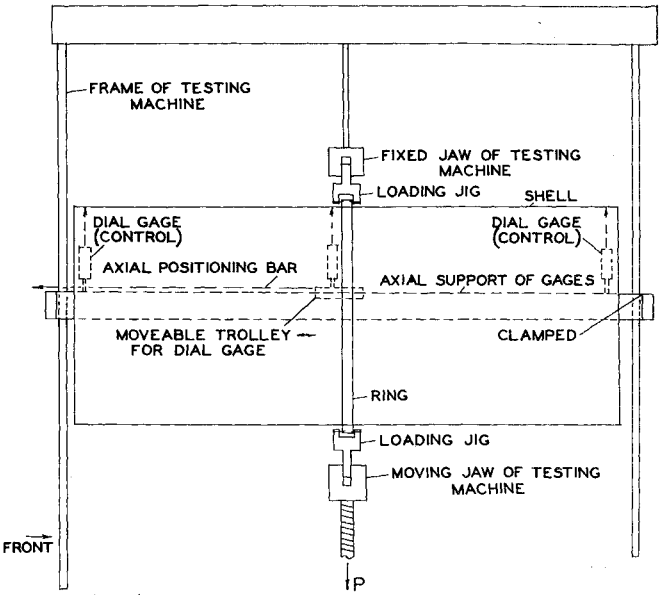

Fig. 1 Test setup (side view). Two end gages are control gages; center gage on moveable trolley is the gage used to measure the radial displacement.

In view of the unexpected behavior of some of the analytical results described previously, the experiment under consideration in this paper was designed. A 30-in. cylinder of mild steel was fabricated from sheet steel of nominal thickness 0.0125 in. An overlap seam was made by a line of spot welds. During the experiment, care was taken to keep this seam 90° from the applied diametral loads. The ring, a T-section, was also mild steel and was spot welded to the cylinder at its midlength.

The geometry of the combined structure is defined by the following: *ring*, $a_r \equiv$ centroidal radius = 5.50 in., $I \equiv$ centroidal moment of inertia of ring cross section = $5.79136(10^{-3})$ in.^{4}, and $A \equiv$ area of ring cross section = .211364 in.^{2}; *shell*, $a \equiv$ mean radius of shell = 5.00 in., $I \equiv$ thickness of shell = 0.0125 in.

In the first experiment the radial deflection of the shell at different locations along a generator was obtained. Dial gages reading to 10^{-4} in. were employed to measure the radial displacement w.

The concentrated loads were applied to the T-section ring by a "jig" and pin arrangement at each end of a diameter (see Fig. 1). Roller bearings were used to eliminate friction so that the applied concentrated loads acted along a diameter. The tongues of the loading jigs were held in the jaws of the testing machine. The supports for the dial gages were rigidly attached to the frame of the testing machine.

Two different arrangements for the dial gages were used. In the first the gases were placed under the top load ($\varphi = \pi/2$). The experiment was then run with the gages at the bottom load position ($\varphi = 3\pi/2$).

Before a run was started, it was necessary to adjust the position of the loading jigs in the jaws of the testing machine so that during the application of the load no rigid body rotation of the shell axis would take place. To eliminate this rotation, control gages (see Fig. 1) were placed at each edge of the shell. Thus, by adjusting the position of the jig in the jaws of the testing machine so that the reading changes in the control gages were the same, a rigid body rotation of the cylinder was eliminated. It was found that once this adjustment was made, the positioning was relatively stable. How-

Received January 29, 1971; revision received May 12, 1971. This investigation was supported by the U.S. Air Force Office of Strategic Research under contract F44620-69-C-0072, Project 9782-01 with the Polytechnic Institute of Brooklyn.

Index categories: Submerged Vessel Systems, Structural Static Analysis.

* Research Group Leader; presently Associate Professor of Mechanical Engineering, Newark College of Engineering. Member AIAA.

† Research Fellow; presently Member of the Technical Staff, Bell Telephone Laboratory, Murray Hill, N. J.

‡ Research Assistant; presently Assistant Professor of Civil Engineering, Newark College of Engineering.

§ Professor and Head, Department of Aerospace Engineering and Applied Mechanics, Polytechnic Institute of Brooklyn. Associate Fellow AIAA.

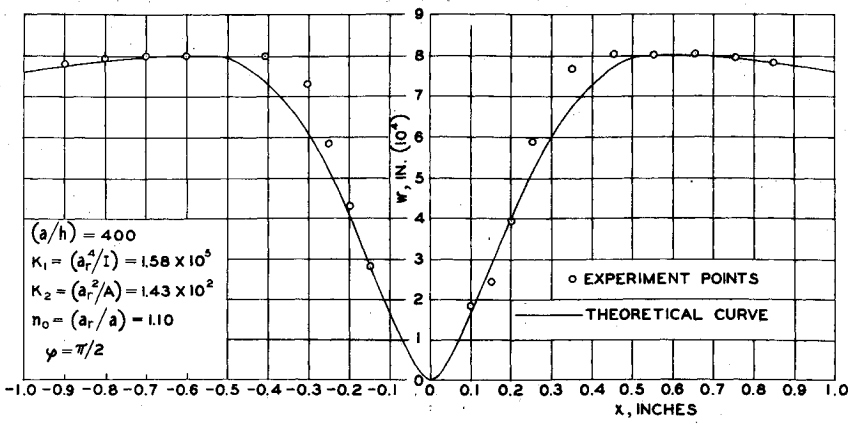

Fig. 2 Radial displacement of shell, $\varphi = \pi/2$ (load = 40 lb).

ever, to hold this setting, a minimum load of 10 lb was always kept on the model.

In order to eliminate a contribution to the deflection readings from irregularities in the surface of the shell, the load at each position was initially zeroed (at the 10 lb setting load), dial gage readings were taken, and then the procedure was repeated at the prescribed loads. The differences in dial gage readings at each position between the setting load and prescribed load conditions were the displacements due to the particular load increment.

The setup of the experiment with the dial gages measuring at $\varphi = \pi/2$ is given in Fig. 1. This position is under the fixed loading jaw. Thus, the dial gage at the ring ($x = 0$, $\varphi = \pi/2$) should give no reading as the load changes. However, this reading does change due to slip in the clamping jaws, flexure of the pins, and other slight deformations of the supporting structure. Thus, the actual displacement at each point of the $\varphi = \pi/2$ generator is not the reading obtained from the dial gage. The reading at $x = 0$, $\varphi = \pi/2$ for each load must be subtracted from the readings, at the same load, for each x position.

In Fig. 2 the radial deflection is plotted vs the position along the $\varphi = \pi/2$ generator of the cylinder. The experimental readings at $x = 0$ have already been subtracted from the readings at each of the stations along the $\varphi = \pi/2$ generator so that the experimental results in Fig. 2 show the true deformation. In the theoretical analysis the cylinder axis was fixed during the deformation, not the point $x = 0$, $\varphi = \pi/2$ which was fixed on the test structure. Thus, in order to compare the theoretical and experimental results, the theoretical deformation at $x = 0$, $\varphi = \pi/2$ was subtracted from all the theoretical data points along the $\varphi = \pi/2$ generator. The curve in Fig. 2 represents the result of this transformation. In the second phase of the experimental work strain gages were mounted along the $\varphi = \pi/2$ generator. The gages were placed so that axial and circumferential strain readings could be taken at both inner and outer surfaces of the shell. In positioning the gages, advantage was taken of the symmetry of the structure and the loading system.

Conclusions

Curves showing the circumferential bending stresses at the inner surface of the shell ($z = h/2$) are given in Fig. 3. Considering these curves, together with the deformed ovular shape, one may question the sign of the stress at the ring ($x = 0$). This stress is positive in the neighborhood of the external load, which seems intuitively incorrect in view of the decrease of the circumferential curvature in this region. However, this seeming contradiction occurs because of a Poisson effect, i.e., the axial bending strain is large enough to determine the sign of the circumferential bending stress. This can be readily seen from Fig. 4, in which the experimental and theoretical bending strains at the inner surface and the membrane strains are plotted along the $\varphi = \pi/2$ generator. From this figure it is quite clear that $0.3\epsilon_{xb}$ is greater than $\epsilon_{\varphi b}$, of opposite sign, and since

$$\sigma_{xb} = E(\epsilon_{xb} + \nu\epsilon_{\varphi b})/(1 - \nu^2), \quad \sigma_{\varphi b} = E(\epsilon_{\varphi b} + \epsilon_{xb})/(1 - \nu_2)$$

determines the sign of the circumferential bending stress.

Figure 3 presents a curve showing the axial bending stress distribution along the $\varphi = \pi/2$ generator. Investigation of the axial bending stresses caused by the concentrated forces indicates that at the load ($\varphi = \pi/2, x = 0$), there is a high tensile stress at the inner surface of the shell. These results also seem to contradict what one would intuitively expect. Why the tensile stress under the load (at $z = h/2$)? Unlike axisymmetrically loaded reinforced cylinders (e.g., a uniform circumferential line load on the ring), the cylinder considered here is subjected to a nonaxisymmetric loading. In fact, for the very significant second harmonic, the tangential component of the interaction load acting on the cylinder and ring is of the order of twice the magnitude of the radial component. We might expect the eccentricity between the shell and ring radii to play a more important role in determining the behavior of the stresses and displacements than in a rein-

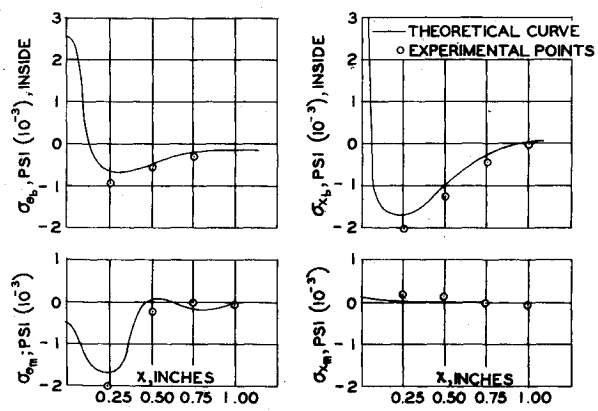

Fig. 3 Stresses in shell, $\varphi = \pi/2$ (load = 40 lb).

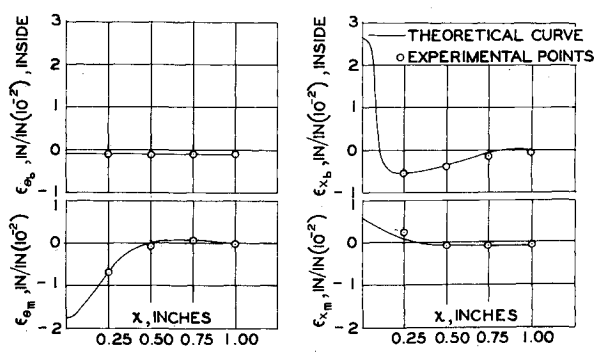

Fig. 4 Strains in shell, $\varphi = \pi/2$ (load = 40 lb).

forced shell loaded axisymmetrically. The effect of the eccentricity is certainly transmitted more directly through the tangential component of the interaction load than through the radial component. Thus, it would appear that the eccentricity together with the nonaxisymmetric loading produce a high tensile axial bending stress (at the inner surface) under the load (see Fig. 3).

The radial displacement curve of Fig. 2 reveals that the maximum radial displacement of the shell does not occur under the ring. The reason for behavior of this nature has already been discussed with respect to the bending stresses. The eccentricity of the ring median line with respect to the shell median surface plays a significant role in determining the response of the structure because the tangential component of the interaction line load is of the same order of magnitude as the radial component. We could, therefore, expect substantial changes in the radial displacement pattern as the eccentricity is varied.

It is clear that the experimental and theoretical results agree sufficiently well to corroborate the unanticipated behavior of the loaded structure.

References

[1] Allentuch, A., Brady, K., and Kempner, J., "Long Cylindrical Shell under Concentrated Loads Applied to a Central Reinforcing Ring," *AIAA Journal*, Vol. 5, No. 10, Oct. 1967, pp. 1863–1870; also PIBAL Rept. 680, Dept. of Aerospace Engineering and Applied Mechanics, Polytechnic Inst. of Brooklyn, N. Y.

[2] Donnell, L. J., "Stability of Thin-Walled Tubes under Torsion," Rept. 479, 1934, NACA.

[3] Hoff, N. J., "Boundary Value Problems of the Thin-Walled Circular Cylinder," *Transactions of the ASME: Journal of Applied Mechanics*, Vol. 76, 1954, pp. 343–350.

[4] Pohle, F. V. and Nardo, S. V., "Simplified Formulas for Boundary Value Problems of the Thin-Walled Circular Cylinder," *Journal of Applied Mechanics*, Vol. 22, No. 3, Sept. 1955, pp. 389–390.

[5] Flügge, W., *Stresses in Shells*, Springer-Verlag, Berlin, 1960, pp. 208–218.

Sonic Boom Minimization Including Both Front and Rear Shocks

A. R. George* and R. Seebass*
Cornell University, Ithaca, N. Y.

THE question of whether flights of supersonic aircraft over populated areas will ever be acceptable depends upon the characteristics of the sonic booms of these aircraft. It is not precisely established which characteristics of a sonic boom signature must be reduced to what levels to make a sonic boom acceptable. For observers outdoors it seems sufficient to reduce the shock strengths of the signature below some substantial fraction of one pound per square foot. For observers indoors, however, the magnitude of the impulse of the signature is also of substantial importance.

The problem of aircraft shaping for minimum front shock strengths taking account of midfield effects was treated by the present authors. The present results extend the analysis of Ref. 1 to treat both front and rear shock strengths. The aircraft weight, effective length, and flight conditions are assumed given and lower bounds for shock strengths are found.

Received May 12, 1971; revision received June 11, 1971. This research was sponsored by NASA Grant NGR-33-010-054.

Index category: Aerodynamic and Powerplant Noise (Including Sonic Boom); Supersonic and Hypersonic Flow.

* Associate Professor, Graduate School of Aerospace Engineering.

The first sonic boom optimization analyses were carried out for the asymptotic far field case of an N wave signature by Jones[2] and Carlson.[3] Later McLean[4] pointed out that nonasymptotic effects could be important and Ferri and Ismail[5] demonstrated significant reductions compared to the far field optimums. Jones,[6] George,[1] and Seebass,[7] then independently derived the nonasymptotic optimums minimizing only Δp_F the front shock pressure jump. These analyses did not treat the rear shock strength Δp_R which in some cases can be much stronger than Δp_F. Later Petty[8] included the condition that the magnitude of the perturbation pressure (not Δp_R) in the rear part of the signature satisfy $|p| \leq \Delta p_F$. He found that the minimums were increased somewhat compared to the front shock optimizations. However, his requirement that $|p| \leq \Delta p_F$ restricts Δp_R to be substantially less than Δp_F and results in quite conservative minimums. He also did not allow for the limiting case of rising pressure in the signature as considered in Refs. 1, 6, and 7. A complete review of sonic boom minimization may be found in Ref. 9.

The present work includes the rear shock strength by requiring $\Delta p_R/\Delta p_F = R \leq R_{\max}$. The number $R_{\max}$ was taken as 1.0 in the minimization calculations. Following the development and notation of Ref. 1, the problem can be formulated as finding the Whitham F function shape which minimizes Δp_F with $R \leq R_{\max}$ and holding the lift

$$L = \left(\frac{8q}{\beta}\right)\int_0^a F(y')(a - y')^{1/2}dy' \qquad (1)$$

constant, where a is the aircraft effective length, q the dynamic pressure and $\beta = (M^2 - 1)^{1/2}$. As discussed in Ref. 1 only the case of lift alone will be treated. The shock strengths are found by inserting shock jumps which hold the area under the nonlinearly advanced F curve constant. The perturbation pressure at the ground for flight at altitude r is then given by

$$p = k_r\alpha\gamma p_g M^2(2\beta)^{-1/2}F/r^{1/2}$$

and the normalized nonlinear advance is defined by

$$m = \frac{2^{1/2}\beta^{3/2}}{\tau(\gamma + 1)M^4}\left(\frac{a}{r}\right)^{1/2} = \left(C_T\frac{a_h}{r^{1/2}}\right)^{-1}\frac{(2\beta)^{1/2}}{\gamma M^3}\left(\frac{a}{r}\right)^{1/2}$$

α, τ, and $C_T a_h/r^{1/2}$ are defined in Refs. 1 and 10 and are 1, 1, and $(\gamma + 1)M/\gamma\beta$, respectively for a uniform atmosphere. k_r is the pressure reflection coefficient of the ground.

Using the nondimensional variable $Y = y/a$, the form of the optimum normalized F function is, for $Y \leq 1$,

$$\mathcal{F} = F/a^{1/2}m = K\delta(Y) + C_1H(Y) + JY - (C_1 + C_3 + J)H(Y - Y_C) \qquad (2)$$

where δ and H are unit impulse and step functions, respectively, and K, C_1, C_3, and Y_C are to be determined. This form

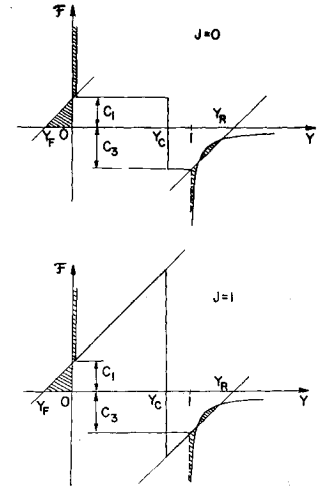

Fig. 1 Optimum $\mathcal{F}$ shapes.